Plane-parallel biases computed from inhomogeneous Arctic clouds and sea ice

Anna Rozwadowska[1] and Robert F. Cahalan

Goddard Space Flight Center, NASA, Greenbelt, Maryland, USA

[1]   Monte Carlo simulations of the expected influence of nonuniformity in cloud structure and surface albedo on shortwave radiative fluxes in the Arctic atmosphere are presented. In particular, plane-parallel biases in cloud albedo and transmittance are studied for nonabsorbing, low-level, all-liquid stratus clouds over sea ice. The "absolute bias" is defined as the difference between the cloud albedo or transmittance for the uniform or plane-parallel case, and the albedo or transmittance for nonuniform conditions with the same mean cloud optical thickness and the same mean surface albedo, averaged over a given area (i.e., bias > 0 means plane-parallel overestimates). Ranges of means and standard deviations of input parameters typical of Arctic conditions are determined from the First International Satellite Cloud Climatology Project (ISCCP) Regional Experiment Artic Cloud Experiment (FIRE/ACE)/Surface Heat Budget of the Arctic Ocean (SHEBA)/ Atmospheric Radiation Measurement Program (ARM) experiment, a cooperative effort of the Department of Energy, NASA, NSF, the National Oceanic and Atmospheric Administration, the Office of Naval Research, and the Atmospheric Environment Service. We determine the sensitivity of the bias with respect to the following: domain averaged means and spatial variances of cloud optical thickness and surface albedo, shape of the surface reflectance function, presence of a scattering layer under the clouds, and solar zenith angle. The simulations show that the biases in Arctic conditions are generally lower than in subtropical stratocumulus. The magnitudes of the absolute biases are unlikely to exceed 0.02 for albedo and 0.05 for transmittance. The "relative bias" expresses the absolute bias as a percentage of the actual cloud albedo or transmittance. The magnitude of the relative bias in albedo is typically below 2% over the reflective Arctic surface, while the magnitude of the relative bias in transmittance can exceed 10%.   *INDEX TERMS:* 0360 Atmospheric Composition and Structure: Transmission and scattering of radiation; 0320 Atmospheric Composition and Structure: Cloud physics and chemistry; 9315 Information Related to Geographic Region: Arctic region; 3250 Mathematical Geophysics: Fractals and multifractals; *KEYWORDS:* SHEBA, FIRE/ACE, plane-parallel bias, cloud trasmittance, cloud albedo, Arctic

1.   Introduction

[2]   The precise modeling of the influence of clouds on radiative fluxes at the surface and in the atmosphere is a crucial problem in climate modeling and satellite remote sensing. Clouds play a unique role in the Arctic energy balance. Clouds over the Arctic Ocean have predominantly a warming effect [*Curry et al.*, 1996]. This is in contrast to lower latitudes, where clouds have a net cooling effect, primarily due to cooling by marine stratocumulus located off the west coasts of the major landmasses (adjacent to Angola, the Azores, California, and Chile/Peru.) Interactions between clouds and seasonal snow coverage are

expected to have a significant effect on Arctic and subarctic climate [*Zhang et al.*, 1996]. Surface-based radiometer data reveal that Arctic stratus clouds produce a net warming of 20 Wm^{-2} in the surface layer during the transition season, suggesting that these clouds may accelerate the springtime melting of the ice pack [*Dong et al.*, 2001]. Solar (shortwave) radiative fluxes are an important component of these interactions.

[3]   A typical approach to the modeling of radiative transfer in Arctic cloudy atmospheres is an assumption of horizontally uniform cloud optical properties [e.g., *Herman and Curry*, 1984; *Zhang et al.*, 1996; *Pinto and Curry*, 1997; *Pinto et al.*, 1997]. However, experimental studies and modeling, carried out outside polar regions, indicate that the large-scale radiative properties of clouds are sensitive not only to the mean cloud characteristics, such as mean cloud water content and effective droplet radius, but also to cloud macrostructure, i.e., its geometry: the distribution of

---

[1]Permanently at Institute of Oceanology, Polish Academy of Sciences, Sopot, Poland.

the cloud sizes, spacings, cloud shapes and aspect ratios, and within-cloud variability [*Cahalan*, 1989; *Barker and Davies*, 1992b; *Cahalan et al.*, 1994a, 1994b; *Zuev and Titov*, 1995; *Byrne et al.*, 1996; *Hignett and Taylor*, 1996]. For layered clouds with relatively high cloud fraction, such as stratus and stratocumulus, the radiative bias due to within-cloud structure typically dominates over that due to "brokenness."

[4] The aim of the present study is to analyze the possible influence of inhomogeneities in cloud structure and in surface albedo on radiative fluxes in the Arctic atmosphere, and to assess the errors introduced by models that neglect the nonuniformity of clouds and sea ice. In particular, this paper focuses on plane-parallel biases in albedo and transmittance for nonabsorbing, low-level, all-liquid stratus clouds over sea ice. The bias is defined as the difference between the cloud albedo or transmittance computed using uniform plane-parallel assumptions with the observed mean cloud optical thickness and surface albedo, and the albedo or transmittance for the actual, nonuniform conditions with the observed mean and variability of cloud optical thickness and surface albedo, averaged over a given area. Note that biases defined above are sums of two components: the "fractal structure" bias and the "independent pixel" bias [cf. *Cahalan et al.*, 1995]. The former is the contribution to the bias from the variable optical thickness of clouds and variable surface albedo by themselves, i.e., under the assumption of the lack of net horizontal photon transport. The latter quantifies how the horizontal transport of photons alters the mean fluxes in nonuniform conditions, and thus isolates the impact of 3-dimensional transport from that due to inhomogeneity alone. We shall assume 100% area coverage by cloud, and thus neglect a third plane-parallel bias component, the "cloud fraction bias," a bias due to cloud "brokenness," known to become significant when cloud fraction is less than about 80%.

[5] Understanding and quantification of the shortwave radiative effect of horizontally inhomogenous stratocumulus clouds over inhomogenous, highly reflective snow/ice surfaces was one of the objectives of the Atmospheric Radiation Measurement Program (ARM)/First International Satellite Cloud Climatology Project (ISCCP) Regional Experiment Arctic Cloud Experiment (FIRE/ACE)/Surface Heat Budget of the Arctic Ocean (SHEBA) joint experiment [*Perovich et al.*, 1999b; *Curry et al.*, 2000]. The ARM/SHEBA experiment was conducted from fall 1997 to fall 1998. The FIRE-ACE was carried out from April to July 1998, during the main experimental phase of the joint experiment. The ARM/FIRE-ACE/SHEBA provided a comprehensive set of sea ice and atmospheric characteristics as well as radiation data, which are employed in this study.

[6] Low level stratus are typical clouds of Arctic summer (May–September) [*Tsay and Jayaweera*, 1984]. Their properties are highly variable from case to case, e.g., in June 1980 shortwave optical depth for the summer low-level Arctic stratus ranged from 2 to 24 [*Herman and Curry*, 1984; *Curry et al.*, 1996]. Liquid water clouds are typical of summer. Based on retrievals from a microwave radiometer and radar measurements, all-liquid clouds, mainly low stratus, occurred 21.6% of the period from May to July 1998 [*Shupe et al.*, 2001].

[7] Cloud fields have been found to have fractal (scaling) properties [e.g., *Cahalan and Joseph*, 1989; *Cahalan and Snider*, 1989; *Davis et al.*, 1996b]. Brightness variations in stratocumulus regions (based on Landsat Thematic Mapper scenes) exhibit a −5/3 power law decrease of the wave number spectra for scales larger than about 200 m, changing to a −3 power at smaller scale [*Cahalan and Snider*, 1989]. This scale break, not observed in power spectra of cloud liquid water, is consistent with horizontal photon transport becoming important at scales equal or less than the radiative smoothing scale [*Davis et al.*, 1997]. Intermittency indices for FIRE and Atlantic Stratocumulus Transition Experiment (ASTEX) clouds are quite similar [*Davis et al.*, 1996b; *Marshak et al.*, 1997]; however, probability distributions of gaps between clouds show that small gaps are significantly more probable in the ASTEX region [*Cahalan et al.*, 1995, see especially Figure 2]. Thus even when the large-scale regime is similar, i.e., subtropical, it can still happen that the structure of cloud fields can depend upon local climatology, for example, more small gaps in the Canaries/Azores region, where there is more convective activity in summer, than in the region off California.

[8] *Cahalan* [1989] and *Cahalan et al.* [1994a, 1994b] used bounded cascade models to reproduce the wave number spectrum and probability distribution of liquid water path (LWP) in marine stratocumulus (Sc). They found the area-averaged albedo of inhomogeneous stratocumulus to be less than that of a uniform cloud with the same microphysical parameters and LWP [see also *Hignett and Taylor*, 1996]. Reduced albedo in inhomogeneous Sc cloud was accompanied by an increase in the transmittance and only a small change in the absorptance. The biases were shown to be generally significant and their dependence on cloud variability, optical depth, scattering albedo and Sun elevation was determined.

[9] Most of the previous studies assumed a black underlying surface, as is appropriate for clouds over a dark ocean. In the Arctic the influence of highly reflective snow and ice surfaces cannot be neglected [e.g., *Pinto and Curry*, 1997]. *Barker and Davies* [1992a] analyzed the applicability of a Lambertian surface and geometric sum formulas for flux calculations in the case of broken cloud fields over a reflecting surface. *Ricchiazzi and Gautier* [1998] showed that the effective albedo which characterizes a given ice distribution is affected by regions well away from the point of interest. Under low clouds (1 km), surface irradiance measurements over snow are significantly affected by the presence of a dark ocean surface more than 7 km away.

[10] Arctic sea ice can be highly nonuniform. The albedo in the visible ranges from about 0.9 for fresh snow to below 0.1 for water. The sea ice bidirectional reflectance distribution function (BRDF) varies from relatively close to Lambertian for fresh snow to almost specular for flat seawater in leads [*Soulen et al.*, 2000; *Arnold et al.*, 2002]. The pattern of the lead network also varies from case to case. The beginning of the melting season further complicates the surface pattern of the sea ice macrostructure. Both ice and snow undergo transformation, which not only changes their albedo but also alters the BRDF. Moreover, melt ponds appear, having reflective properties that are modified by the underlying ice, thus differing from those of deep water [e.g., *Grenfell and Perovich*, 1984; *Allison et al.*, 1993; *Grenfell*

et al., 1994; *Perovich*, 1994, 1998; *Perovich et al.*, 1999a; *Arnold et al.*, 2002].

[11] *Benner et al.* [2001] examined plane-parallel biases in albedo and transmittance for cases chosen from the FIRE-ACE/SHEBA period (21 July and 18 May 1998). They found that both cloud and surface inhomogeneity had only a small impact on domain average fluxes. However, their study was based on only two cases. In both cases clouds were optically very thin (mean optical thickness of 6.7 and 2.2 for May and July cases, respectively). Moreover, they determined the variance of surface albedo from statistics of melt ponds and open water derived from downlooking video images, so that actual surface albedo variability may have been underestimated.

[12] In the present study we analyze the possible influence of nonuniform cloud structure and nonuniform surface albedo on radiative fluxes in the Arctic atmosphere, focusing on plane-parallel biases in cloud albedo and transmittance. We do not intend to analyze any particular case but rather estimate the maximum bias to be expected, and specify the conditions for which a maximum bias may be expected. The analysis is based on Monte Carlo simulations. Ranges of means and standard deviations of input parameters typical of Arctic conditions are obtained from the FIRE-ACE/SHEBA/ARM experiment. We assume fully overcast sky. This is justified by the approximately bimodal distribution of Arctic cloud cover. The Arctic sky is usually either clear (0–2 tenths) or overcast (8–10 tenths) [*Makshtas et al.*, 1999]. The dependence of the bias is studied with respect to several factors, including: domain averaged values and spatial variability of the cloud optical thickness and surface albedo, shape of the surface reflectance function, presence of a subcloud scattering layer, and solar zenith angle.

[13] The outline of the paper is as follows: Section 2 describes the FIRE-ACE/SHEBA/ARM data applied in this study: cloud LWP and auxiliary cloud data as well as reflected radiances over sea ice. Section 3 describes "tuning" the bounded cascade model to produce a distribution of cloud LWP appropriate for the Arctic stratus observed in SHEBA, and also presents the technique used to simulate spatial variability of surface albedo based on sea ice observations during SHEBA. Also in section 3 is a brief description of the Monte Carlo radiative transfer method employed here, and a summary of cloud cases analyzed. Section 4, "Results", presents and discusses the plane-parallel bias computed from the cloud/ice distributions, and the dependence of these biases on various factors, e.g., domain averaged values and spatial variability of cloud optical thickness and surface albedo, shape of the surface reflectance function, presence of a subcloud scattering layer, and solar zenith angle. Section 5, "Conclusions", summarizes our findings and discusses possible future research arising from this study. Finally, Appendix A discusses the sensitivity of the bias to model parameters, with the help of simple analytical expressions.

2. Data
2.1. Clouds

[14] LWP data are used in this paper to characterize the spatial inhomogeneity of Arctic low-level liquid clouds.

They were obtained from ground-based microwave radiometer (MWR) measurements taken at the SHEBA ice station in the period of April to June 1998, as part of the ARM sponsored by the U.S. Department of Energy. The microwave radiometer used at SHEBA is a Radiometrics WVR-110 with receivers at 23.8 and 31.4 GHz. Brightness temperatures measured by the radiometer were used to derive the LWP in 1.9-min intervals [*Shupe et al.*, 2001]. Because of significant discrepancies between the radiometer-derived LWPs and the estimates from aircraft in-situ measurements, the original data were reprocessed by NOA AETL (Environmental Technology Laboratory), using more recent data on the dielectric constants of supercooled water. The reprocessing diminished the difference. Details of reprocessing are given by *Westwater et al.* [2001]. The value of 30 g m^{-2} is the theoretical accuracy of the retrievals but values below this threshold can still indicate liquid water if the clear sky baseline is observed to be at a lower value (M. D. Shupe, personal communication, 2001).

[15] Our analysis is limited to low-level liquid clouds and selection was aided by additional information indicating times when only low-level all-liquid clouds or low-level all-liquid clouds accompanied by higher ice clouds were present (M. D. Shupe, personal communication, 2001). Phase determination was made by NOAA ETL for each case separately by examining MWR-derived LWPs, infrared radiometer brightness temperatures, the structure of radar reflectivities and Doppler velocities, lidar depolarization ratios, and temperature and humidity profiles from radiosondes [*Shupe et al.*, 2001]. The heights of cloud tops and bases determined from 35 GHZ radar measurements (every 10 s), the radar and Depolarization And Backscatter Unattended Lidar (DABUL) images, all available from the CODIAC database, as well as surface meteorological reports from the SHEBA station, provided addition information on cloud structure and weather conditions. For a description of the NOAA ETL radar and lidar operated during SHEBA see, e.g., *Shupe et al.* [2001], and the CODIAC database documentation.

2.2. Sea Ice

[16] To simulate variable sea ice albedo we used reflected radiances from a MODIS Airborne Simulator (MAS) [*King et al.*, 1996] measured during a flight over sea ice. MAS has relatively small pixel size (50 m in the nadir; the ground distance between the centers of the scan lines is 33 m) and scenes cover relatively large areas. The only day when MAS mapped sea-ice surfaces comes from the premelting period (20 May 1998, track #12, channel 1; data from G. T. Arnold and J. Y. Li, private communication). The lead network, however, is already detectable. Figure 1 shows a 66-km-long fragment (2000-pixels) of this scene.

3. Models and Input Parameters
3.1. Bounded Cascade Fractal Model and Arctic Clouds

[17] Previous study showed that the bounded cascade model reproduced well the probability distribution and power spectrum of liquid water path (LWP) in a nonuniform stratocumulus cloud in midlatitudes [*Cahalan*, 1989; *Cahalan et al.*, 1994a, 1994b]. In this paper, the bounded cascade

Figure 1. Fragment (716×2000 pixels) of the Arctic sea ice MAS image (20 May 1998, track #12, channel #1), used in the simulation of sea ice albedo variability.

is used to simulate LWP variability in Arctic stratus for the purpose of estimating plane-parallel bias. The model LWP distribution is lognormal-like near the mean but vanishes outside a finite range. The bounded cascade also produces a power law wave number spectrum, similar to those observed in ASTEX and FIRE. The model is characterized by two parameters: the variance parameter, f, related to the standard deviation of $\log_{10}$(LWP) and the scaling parameter c, related to the exponent of the power spectrum (or slope on a log-log scale) of the LWP. For given parameters c and f, at the cascade step n, each cell is divided into two equal parts and fraction $0 \leq f \cdot c^n \leq 1$ of liquid water is randomly transferred from one half to the other. For the concept and the properties of cloud bounded cascade model, see *Cahalan* [1994], *Cahalan et al.* [1994a], and *Marshak et al.* [1994]. Further in the paper, log(LWP) will denote $\log_{10}$(LWP).

[18] We used LWP time series to choose the bounded cascade model parameters best fitting the Arctic data. Using the information on cloud phase, heights of cloud tops and bases, the radar and DABUL images, we selected cases of all-liquid low-level clouds with bases less than 1000 m above the ice surface. These clouds can be accompanied by higher all-ice cloud. The LWP data were discarded if the quality flag was raised, mainly due to wetting of the instrument window from precipitation. However, all other LWP measurements, even those taken when surface observers reported fog or precipitation, were included in our data set. Ice precipitation from all-liquid clouds was observed quite often during Arctic summer (M. D. Shupe, personal communication, 2001). Ice crystals do not bias MWR measurements. As for fog, it can be treated as a stratus cloud with base approaching the sea ice surface.

[19] Forty-six cases of 6-hour LWP series for all-liquid water clouds were selected for the analysis of the horizontal LWP distribution and tuning the bounded cascade model to Arctic conditions. In 29 of these cases radar showed 100% coverage with low-level clouds; in 45 the radar detected low-level clouds for at least 90% of the time. In one case only, the mean low-level cloud cover was about 74%. Typically, the low clouds were coded as "stratus in a more continuous sheet or layer, or in ragged shreds or both, but no ragged stratus of bad weather." There were also individual observations of stratocumulus and cumulus reported. Fog obscuring the sky was reported at least once during 15 out of 46 6-hour cases.

[20] We used LWP time series but time variability can be converted to space variability by assuming frozen turbulence, i.e., by the assumption that the variations in cloud LWP observed at the SHEBA station are mainly due to advection of the spatial pattern of the turbulent liquid water field, rather than to local time dependence of the field [*Cahalan and Snider*, 1989]. The wind speed at the cloud level obtained from tethered balloon soundings from the SHEBA site and from NCAR C-130 vertical profiles typically ranged from 3 to 9 m/s with the mode at 5 m/s (for the all-liquid low-level cloud cases for which soundings are available). Taking the advection velocity as 5 m/s, the spatial scales of our analysis are 570 m to 108 km. Unfortunately, the smallest scale is too large to resolve the fine structure of the clouds. The extrapolation of the variance of log(LWP) obtained for the scales $0.57-108$ km to the scales $0.033-67$ km is justified by the scaling behavior of both the real stratiform clouds and the bounded cascade clouds. Taking the actual slope of log(LWP) power spectrum in log-log scale for the FIRE-ACE/SHEBA cases ($-1.3--1.4$) the variance from the scale range $0.57-67$ km is about 80% of the variance for the scale range $0.033-$
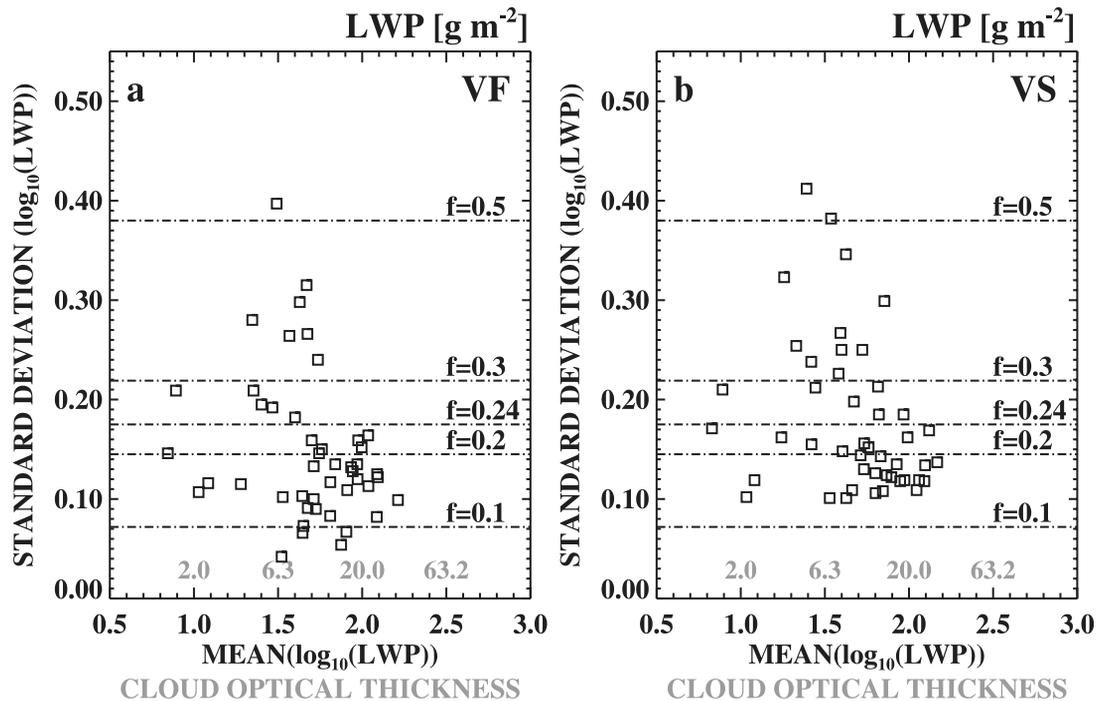
Figure 2. Mean and standard deviation of log(LWP) for low-level, all-liquid clouds in the Arctic (SHEBA station, April–July 1998), calculated for 6 hour-long series of MWR measurements by VF (a) and VS (b) methods. Cloud optical thickness marked on the *x* axis was calculated for a constant droplet diameter 7.5 μm.

67 km. However, the variances for the ranges 0.033–67 km and 0.57–108 km are very close.

[21] The parameters of the bounded cascade fractal model were calculated for each 6-hour LWP series for all-liquid water clouds. Methods for parameter estimation are given by *Cahalan et al.* [1994a]. To calculate the fractal parameter *f* from MWR LWP measurements, *Cahalan et al.* [1995] rejected all measurements below a threshold equal to 10 g m^{-2}, and determined ⟨log(LWP)⟩ and $\sigma_{\log(LWP)}$ by fitting a Gaussian curve to a histogram of log(LWP), where the mean, indicated in this paper by angular brackets ⟨ ⟩, the standard deviation, σ, and the norm (integral of the Gaussian) were freely varied so as to minimize χ^2 in the usual way for a histogram. Assuming the real distribution is lognormal, this method gives good estimators of the distribution even if the threshold eliminates a considerable number of observations. However, an application of this method to the SHEBA measurements resulted in rejecting several 6 hour-long LWP series because the majority of the observations in these series were below the threshold.

[22] In this work, a threshold was determined individually for each time series such that the percentage of the observations above the threshold equals the percentage of the time when the radar detected low-level clouds, i.e., cloud base and top was determined (CODIAC database). We used two methods for estimation of log(LWP) standard deviation. In the first one (later referred to as VF: Variable threshold, parameters determined by Fitting), the $\sigma_{\log(LWP)}$ estimate was calculated by the fitting method. In the second method VS (Variable threshold, parameters determined directly from Sample) the estimate was computed directly from the sample, as $\sigma_{\log(LWP)}$. If the real distribution is close to

lognormal, "fitting" and "sample" methods give very close results. Otherwise, the fitting method gives a distribution that fits better to the mode of the histogram than the sample method but "ignores" its usually lower tail, where the number of observations is relatively low. Both methods are likely to include all the individual LWP measurements for the cloudy parts of the 6-hour series, even those from very thin parts of the cloud. However, estimates calculated with VS can be biased by noise because the histograms contain data with values much below the noise level of the LWP retrieval method. VF often misses the lower tail of the distribution, and this is likely to be most significant when many of the sampled values lie near or below the threshold. The equation $\sigma_{\log(LWP)} = 0.718f(1 - 0.556f^2)/(1 - 0.720f^2)$ approximates the relationship between $\sigma_{\log(LWP)}$ and *f* [*Cahalan*, 1994].

[23] Means and standard deviations of log(LWP) are plotted in Figures 2a and 2b for each histogram and for VF and VS methods, respectively. Figure 2 shows that regardless of the estimation method, Arctic low-level liquid water clouds are much less variable than midlatitude stratocumulus. The standard deviation of log(LWP) usually does not exceed 0.3. For cloud cases with high $\sigma_{\log(LWP)}$ the radar image usually shows considerable changes in cloud thickness, in reflected signal, or in cloud height. This happens, e.g., when the cloud field develops, dissipates (changes in time) or on the edges of the field (advection). The bounded cascade variance parameter *f* ranges from 0.1 to 0.4. For comparison, the diurnal mean fractal parameter was about 0.6 in ASTEX and about 0.5 in FIRE [*Cahalan et al.*, 1995]. The difference is considerable even if we account for the difference in the methods. Unlike in this paper,
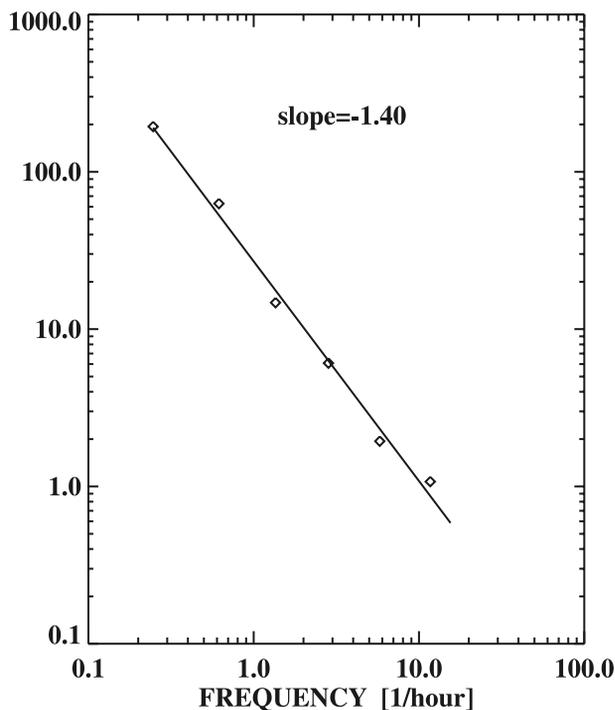
slope=-1.40

Figure 3. Binned averaged power spectrum for cloud LWP retrievals (symbols) and corresponding least squares straight line fit with slope −1.40, from the SHEBA station for April through July 1998 for all cases of low-level all-liquid clouds.

parameters for ASTEX and FIRE were calculated from the averaged or "long-term" histograms (28 and 18 days, respectively; the respective shortest scales equal 1 and 0.5 min) and the threshold of 10 g m^{-2} was applied to the LWP data. The parameter f computed from the composite histogram for all the LPW data analyzed in this study is about 0.4, still significantly lower than in FIRE and ASTEX. One of the reasons for relatively low variability in LWP in Arctic low level stratus clouds can be the humidity inversion above the cloud topped mixed layer, rare outside the polar regions, which appears to contribute to the homogeneity and persistence of the cloud deck by inhibiting evaporative cooling associated with entrainment mixing at cloud top [*Curry et al.*, 2000].

[24] LWP power spectra were computed for each low-level liquid cloud case and averaged. To prevent high frequencies from dominating the spectral slope fitting, the averaged spectrum was binned into increments of length increasing as 2^n. Such logarithmic binning distributes spectral values almost equally on a log-log scale. The spectral exponent is determined by fitting a line to the binned spectrum on a log-log scale.

[25] The exponent of the power spectrum averaged over all low-level liquid cloud cases is −1.40 ± 0.06. The binned spectrum and fitted line are given in Figure 3. The slope obtained for SHEBA is similar to averaged slopes reported for ASTEX (PVM-100 probe) and FIRE 87 (King LWC probe): −1.43 ± 0.08 (scales from 60 m to 60 km) and −1.36 ± 0.06 (scales from 20 m to 20 km), respectively [*Davis et al.*, 1996b]. Differences in the range of available

scales in FIRE, ASTEX and SHEBA should not influence the respective LWC or LWP spectral exponents. *Davis et al.* [1999] found that the large-scale LWC power spectrum is represented by the same power exponent down to scales of several meters. The scales of the power spectrum from ASTEX, FIRE, and SHEBA/FIRE-ACE are above this scale.

[26] The slope may vary from realization to realization reaching also −5/3, the value for an "upscale cascade" in 2D turbulence [*Kraichnan*, 1967; *Gage and Nastrom*, 1986; *Cahalan and Snider*, 1989]. Values near this theoretical slope were observed, e.g., for MWR LWP measurements from FIRE 87. The fractal parameter is related to spectral slope α as $c^2 = 2^{(1 - |\alpha|)}$. For slope $\alpha = -5/3$ this gives c = $2^{(-1/3)} \sim 0.8$, while slope $\alpha = -1.40$ gives c = 0.87.

[27] Plane-parallel bias simulations presented in this paper use scaling parameter $c = 0.8$ and variance parameter $f = 0.24$. $f = 0.24$ is equal to $\langle f \rangle$ for all 6-hour cases and VS method of $\sigma_{\log(\text{LWP})}$ determination. $\langle f \rangle$ obtained by the means of VF method is about 0.2. Because of the typically low variability of LWP in Arctic clouds, usage of the bounded cascade representation of the LWP distribution in simulations should not introduce much error. However, the problem to what extent Arctic clouds are scaling fractals needs further study.

3.2. Ice Albedo Simulations

[28] Unfortunately, the only day when MAS mapped sea-ice surfaces comes from the premelting period and is characterized by high mean albedo and low variability (20 May 1998, track #12, channel 1; data from G. T. Arnold and J. Y. Li, private communication). To determine parameter sensitivity in bias simulations, a wide range of sea ice surface states is needed, with different values in both the mean and the standard deviation of the albedo. To obtain this range of states, 5 transects along the flight were selected from the MAS scene. Then each transect (67.5 km long) was transformed to obtain four different cases: transects with mean albedos 0.5 and 0.8 and standard deviations 0.15 and 0.25. For comparison, the mean surface albedo at the SHEBA station (for $\lambda = 605$ nm) measured along a 200 m-long "albedo line" varied from 0.95 ($\sigma_{As} = 0.01$) in April, to 0.5 ($\sigma_{As} > 0.25$) in the peak of the melting period [*Perovich et al.*, 1999a]. To obtain a surface albedo series with the mean albedo equal to 0.8, the MAS scene was transformed as follows: two thresholds were chosen, and points with albedo greater than the upper threshold were assigned albedo = 0.95 to agree with the albedo of fresh snow at 605 nm [see *Perovich et al.*, 1999a], while points with albedo below the lower threshold were assigned albedo = 0.1, typical of ice-free water. Points between the thresholds were transformed linearly. Thresholds were chosen individually for each transect and each case to obtain desired values of the mean and standard deviation of the albedo. The transformation for the cases of the mean equal to 0.5 was similar, except that the albedo assigned to points above the upper threshold becomes 0.72 (close to albedo of white ice for $\lambda = 605$ nm; compare, e.g., *Perovich et al.* [1999a]). Figure 4a shows an example of the albedo series before and after the transformation.

[29] The transformation does not change the original character of the power spectrum (Figure 4c), with exponent between 0 and −1, and keeps the realistic (bimodal) shapes
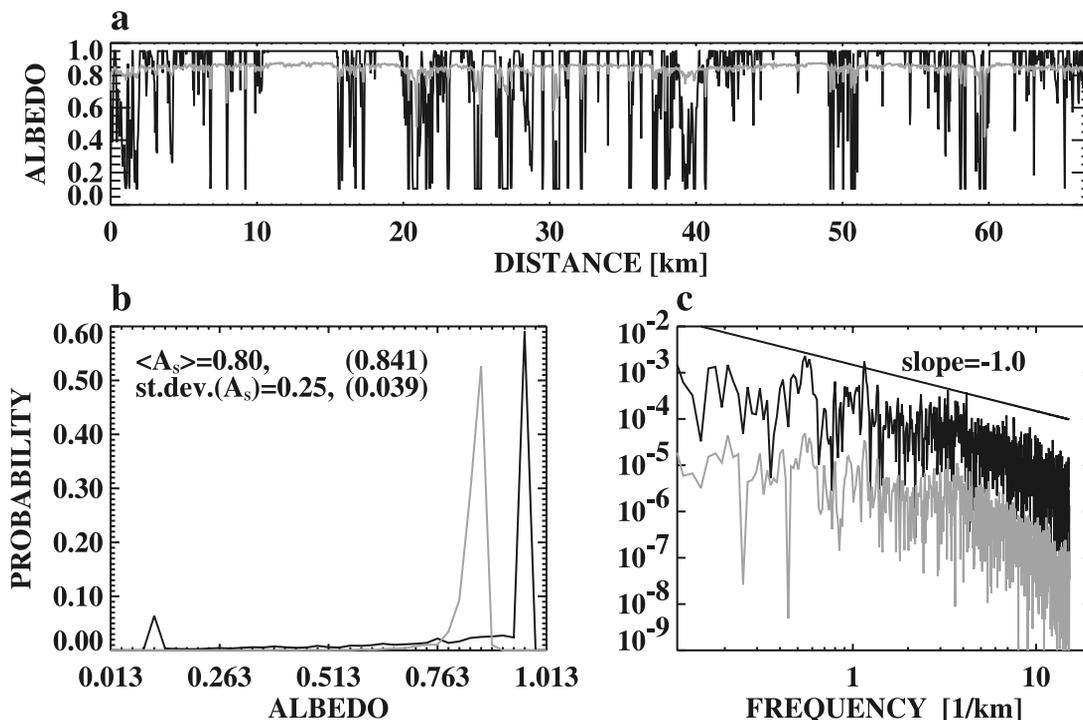
Figure 4. Example of sea ice albedo simulation:
1. original (gray line) and transformed (black line) transects of sea ice albedo (reflectance),
2. histogram of the original and transformed data
3. power spectrum of the original and transformed albedo (reflectance) transects.

of the albedo histograms (Figure 4b). The break in the spectral slope at about 3 km^{-1} may come from the possible presence of thin cirrus. Under the assumption that the threshold for separating lead albedo from ice albedo is 0.3, the lead cover in our transformed surfaces varies from 3% for mean surface albedo $A_s = 0.8$ and standard deviation $\sigma_{As} = 0.15$, to 28% for $A_s = 0.5$ and $\sigma_{As} = 0.25$. For comparison, lead cover during SHEBA varied from several percent to about 18% in August [*Perovich et al.*, 1999a]. The spatial distribution of the resulting simulated ice albedo resembles strongly cracked ice.

3.3. Radiative Transfer Model

[30] Radiative transfer was simulated by a 3D Monte Carlo code developed by *Marshak et al.* [1995], using the "maximum cross-section method" of *Marchuk et al.* [1980]. All simulations were performed for $\lambda = 605$ nm. A 300 m thick cloud layer is assumed to have its base 150 m above the reflective surface. The space between the cloud sheet and the surface is usually "empty" in our simulations, except in one experiment in which clouds and surface are separated by a nonabsorptive scattering layer with scattering coefficient 0.1, 0.01, or 0.001 and asymmetry factor of the scattering function 0.68. Clouds are also nonabsorptive with asymmetry factor 0.85 (for $\lambda = 605$ nm). Mean cloud optical thickness, $\langle \tau \rangle$, varies from 1 to 30, but the majority of calculations were performed for $\langle \tau \rangle = 15$. Assuming an effective droplet radius equal to 7.5 μm, these correspond to LWP varying from 5 to 150 g m^{-2}. For comparison, a mean droplet equivalent radius for low-level Arctic clouds ranges from 7.5 to 7.8 μm in June [*Curry et al.*, 1996; *Hobbs and Rangno*, 1998], 7.4 μm in April–July 1998 [*Shupe et al.*, 2001], and 9.7 μm in early autumn [*Pinto et al.*, 2001]. Variability in LWP is simulated by the bounded cascade fractal model with variance parameter typically 0.24 and spectral (scaling) parameter 0.8.

[31] Mean surface albedo in the simulations is set to 0.0, 0.5 and 0.8 with standard deviation 0.0 (uniform case), 0.15 and 0.25 ("standard case"). The surface reflection function is usually assumed lambertian, except for an experiment in which the sensitivity of the fluxes on the shape of the surface reflectance function are investigated. The surface albedo variability is simulated by the transformed transects from the MAS scene, a fragment of which is shown in Figure 1.

[32] Cloud liquid water path and surface albedo are variable in 1D, along the same horizontal direction. Photons travel in 3D space. For uniform (plane parallel) cases, single runs with $2*10^7$ photons were performed. For nonuniform cases, 5 runs were conducted for each case, each with $2*10^7$ photons. The length of the domain is 67.5 km. The smallest uniform distance (minimum "pixel" size) is 0.033 km. Solar zenith angle 60° is taken as the "standard" value. For the full list of the numerical experiments performed and their input parameters see Table 1.

[33] Our assumption on 1D variability in sea ice albedo and cloud optical thickness should only mildly affect the biases obtained. Previous work showed that the horizontal photon transport effect in overcast clouds over a dark surface is small compared to the optical depth variability effect in the domain average [e.g., *Cahalan*, 1994; *Cahalan et al.*, 1994a, 1994b]. Horizontal photon transport is expected to be more important in cloud over a reflective

Table 1. List of Numerical Experiments Performed to Study Plane-Parallel Biases in the Arctic, and Their Input Parameters[a]

Type of Numerical Experiment	Cloud Optical Thickness	Bounded Cascade Variance Parameter	Scale of Variability in Cloud, km	Surface Type	Mean Albedo	Albedo Standard Deviation	Scale of Albedo Variability, km	Cloud Height, km	Solar Zenith Angle, deg	Scattering Coefficient of the Atmosphere, km^{-1}
Biases v. $\langle\tau\rangle$	5–30	0.24	uniform, 0.033	lambertian	0, 0.5, 0.8	0.25	uniform, 0.033	0.150	60	0
Biases v. ϑ	1, 15	0.24	uniform, 0.033	lambertian	0, 0.5, 0.8	0.25	uniform, 0.033	0.150	10, 40, 60, 80	0
Biases v. variability in τ	15	0, 0.24, 0.4, 0.5	uniform, 0.033	lambertian	0, 0.5, 0.8	0.25	uniform, 0.033	0.150	60	0
Biases v. variability in A_s	15	0.24	uniform, 0.033	lambertian	0.5, 0.8	0, 0.15, 0.25	uniform, 0.033	0.150	60	0
Biases v. type of surface scattering	5, 15, 25	0.24	uniform, 0.033	lambertian mirror	0.5, 0.8	0.25	uniform, 0.033	0.150	60, 80	0
Biases v. cloud base height	15	0.24	uniform, 0.033	lambertian	0.5, 0.8	0.25	uniform, 0.033	0.075, 0.150, 0.300, 0.600, 1.200	60	0
Influence of scattering layer under clouds on biases	5, 15	0.24	uniform, 0.033	lambertian	0, 0.5, 0.8	0.25	uniform, 0.033	0.150	60	0, 0.001, 0.01, 0.1
Influence of τ-A_s correlation on biases	15	0.24	0.033	lambertian	0.5, 0.8	0.25	0.033	0.150	60	0

[a] τ and ϑ are cloud optical thickness and solar zenith angle, respectively. "Scale of variability" is the largest uniform area in a given run. For a uniform case, it equals 67.5 km.

surface system, due to multiple reflection between the clouds and the surface. However, our simulations show that cloud albedo and transmittance are sensitive to the correlation between the surface albedo and cloud optical thickness variabilities, which may suggest that the horizontal photon transport is relatively small also in Arctic conditions. Therefore using 1D variability in clouds and in the underlying surface is likely to be adequate for overcast clouds over sea ice. Moreover, stratiform clouds with nearly 1D variability are observed (kind "undulatus"). Similarly, leads can have privileged direction depending on sea ice dynamics.

[34] A Monte Carlo model based on the maximum cross-section method has been compared successfully with other radiative transfer models for several 3-dimensional stratiform and convective cloud fields as part of the International Intercomparison of 3-dimensional Radiation Codes (I3RC; see http: i3rc.gsfc.nasa.gov). For the special case of uniform clouds, it was also tested against DISORT [*Stamnes et al.*,1988, 2000] for a wide range of plane-parallel cloud parameters. Absolute differences between albedos and transmittances calculated by both methods do not exceed 0.001.

4. Results

[35] In this section we describe plane-parallel biases in albedo and transmittance, and their dependence on the mean and variance of cloud and surface properties, at solar zenith angles appropriate for Arctic conditions. We focus on two shortwave radiative fluxes in the Arctic atmosphere: downwelling irradiance at the sea surface, expressed as atmospheric (cloud) transmittance T, and upwelling irradiance at the top of clouds, expressed as cloud albedo above clouds A, and their plane-parallel biases. The absolute bias is defined as the difference between the cloud albedo or transmittance for the uniform or plane-parallel case, and the albedo or transmittance for the actual, nonuniform conditions with the same mean cloud optical thickness and the same mean surface albedo, averaged over a given area:

$$\Delta A = A_{PP}(\langle\tau\rangle, \langle A_s\rangle) - A \qquad (1)$$

$$\Delta T = T_{PP}(\langle\tau\rangle, \langle A_s\rangle) - T \qquad (2)$$

Note that $\Delta A > 0$ means that the plane-parallel assumption overestimates A. As was mentioned in the introduction, the plane-parallel biases defined above are the sums of two components: the "fractal structure" bias and the "independent pixel" bias.

[36] The biases are analyzed for mean cloud optical thickness ranging from 1 to 30. The results for $\langle\tau\rangle$ from 5 to 30 are presented in Figure 5. Variability in cloud optical thickness only (i.e., constant A_s) results in lower cloud albedo measured above clouds, when compared to the plane-parallel case with the same mean cloud optical thickness, so that the cloud contribution to the albedo bias $\Delta A_\tau > 0$. In the case of nonreflective surface, such as ocean, the magnitude of the albedo bias ΔA_τ for Arctic clouds is much lower than that observed in midlatitudes, e.g., during ASTEX and FIRE [*Cahalan et al.*, 1994a; *Cahalan et al.*, 1995] and it typically does not exceed
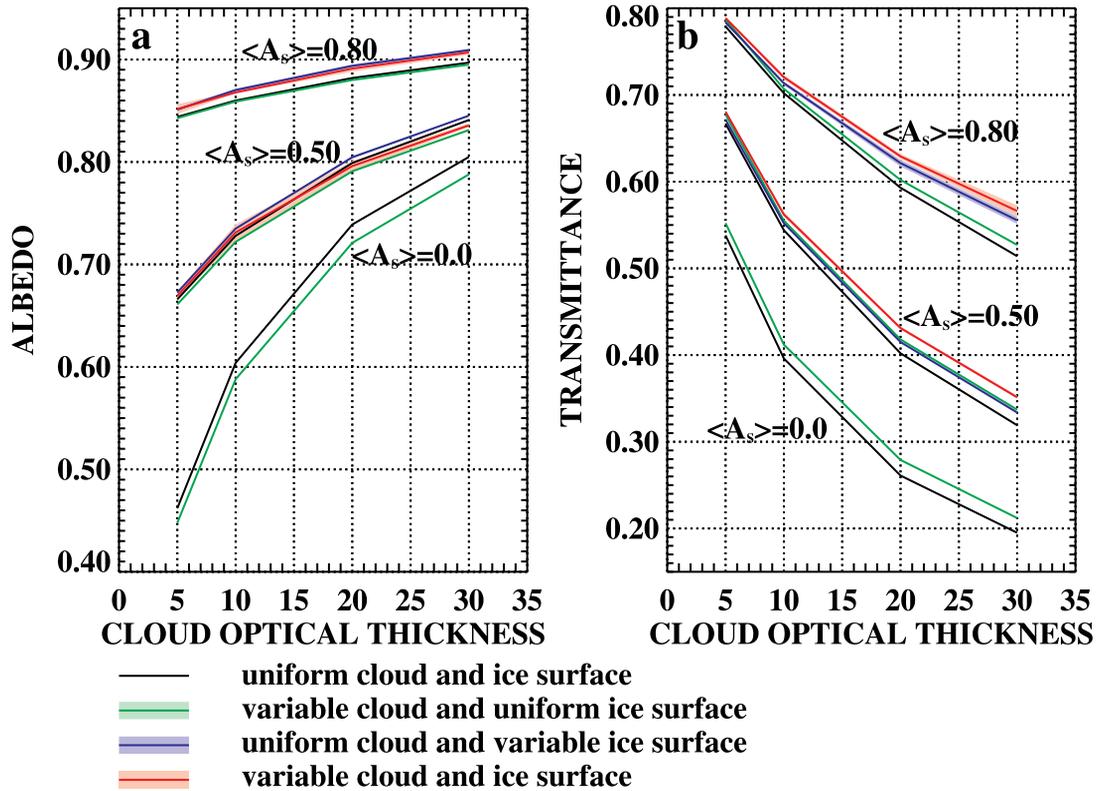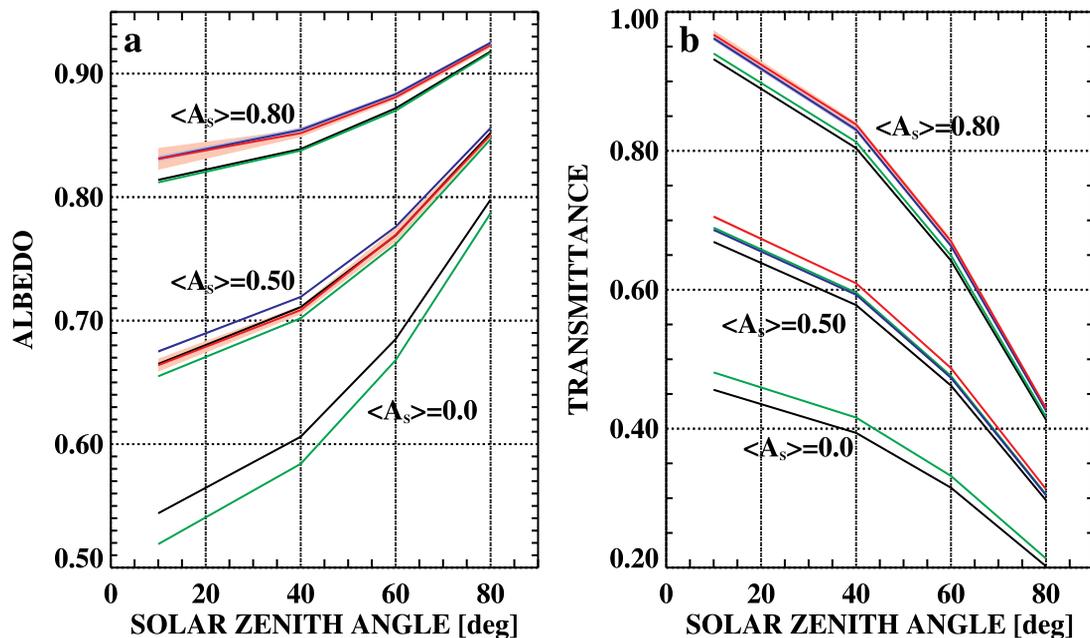
Figure 5. Biases in cloud albedo and transmittance versus mean cloud optical thickness for $\vartheta = 60°$, $f = 0.24$, $\sigma_{As} = 0.25$. Black curves denote plane-parallel cases. Red curves denote cases when both surface and clouds are variable. Green curves denote cases with variable cloud optical thickness only and blue curves cases with variable surface albedo. Mean values of cloud albedo and transmittance (curves), and their standard deviations (shades polygons) calculated from 5 runs, each run for a different realization of A_s and τ, are given for each case.

0.02 in the Arctic. This is due to much lower variability in cloud optical thickness in the Arctic. For comparison, in ASTEX, the fractal structure bias for albedo exceeded 0.1 in its diurnal cycle. As the plane-parallel bias contribution due to domain averaged horizontal photon transport in ASTEX was usually almost negligible, the fractal structure bias was approximately equal to the plane-parallel bias defined in this paper. An increase in the mean surface albedo results in a decrease in ΔA_τ because increased upwelling radiation from the surface partly compensates the decreased cloud albedo in the thin cloud regions, which results in smaller changes in actual measured albedo, and thus the albedo bias over a reflective surface is also smaller. Cloud albedo has two contributions: the flux reflected upward directly by the cloud, and also the flux transmitted through it, once or multiply reflected between surface and cloud, and eventually transmitted upward through the cloud (compare (A5)). For a highly reflective uniform surface (e.g., snow) ΔA_τ practically equals zero. The transmittance bias due to cloud nonuniformity, ΔT_τ is negative. Its magnitude does not exceed 0.02. ΔT_τ is also much lower in the case of a highly reflective underlying surface than it is for a dark surface. Increased downwelling radiation in thin cloud regions is partly compensated by decreased cloud albedo for the upwelling flux from the surface, so that actual transmittance, i.e., the transmittance including the multiple reflected flux, changes little (compare (A6)). The magnitudes of both

ΔA_τ and ΔT_τ increase with the increase in the mean cloud optical thickness.

[37] A variable reflective surface (Figure 5) results in increasing both albedo above clouds and atmospheric transmittance when compared to the plane-parallel case with the same mean value of the surface albedo, i.e., ΔA_{As} and $\Delta T_{As} < 0$. Surface properties influence albedo and transmittance, and related biases, by multiple reflection between cloud and surface, which results in nonlinear hyperbolic terms in the respective equations (compare (A5) and (A6)). In the case of uniform clouds over a highly nonuniform and reflective surface ($\langle A_s \rangle = 0.8$, $\sigma_{As} = 0.25$) with solar zenith angles typical of the Arctic, the absolute value of the albedo bias ΔA_{As} is below 0.02, while the transmittance bias (ΔT_{As}) magnitude can reach 0.04 for optically thick clouds. Within the analyzed ranges of parameters, magnitudes of both biases slightly increase with an increase in mean cloud optical thickness, except for low surface albedo ($\langle A_s \rangle = 0.5$) when $|\Delta A_{As}|$ is maximum for $\langle \tau \rangle$ of about 10–15.

[38] The total biases $\Delta A_{\tau,As}$ and $\Delta T_{\tau,As}$ (cloud and surface variable) are the sum of both bias contributions, due to cloud optical thickness and surface albedo variability. In the case of albedo bias both contributions tend to compensate for each other (Figure 5), so the total bias can be positive or negative depending on which contribution dominates. Considerable $\Delta A_{\tau,As}$ can be expected for the cases of variable clouds over the dark sea, e.g., open water

Figure 6. Biases in cloud albedo and transmittance versus solar zenith angle for $\langle\tau\rangle$ = 15, f = 0.24, σ_{As} = 0.25. See Figure 5 for explanation of line patterns.

or initial freezing stages, when the cloud bias contribution dominates, or for clouds over a variable surface with high albedo, when the surface component dominates. The value of $\Delta A_{\tau,As}$ does not exceed ±0.02. The more reflective the ice is, the less the cloud variability influences the albedo bias. In the case of transmittance, both contributions are negative. The highest $|\Delta T_{\tau,As}|$ in this simulation, exceeding 0.05, is found for $\langle A_s\rangle$ = 0.8 (the highest $\langle A_s\rangle$ analyzed), thick cloud and the highly variable surface. For the modeled conditions, increased cloud optical thickness has a negligible effect on the total albedo bias, but may increase the transmittance bias magnitude up to several times.

[39] Figure 6 presents the influence of solar zenith angle on the biases. In the Arctic, i.e., north of the Polar Circle, solar zenith angle is never lower than 47° with typical summer values from 43° to 80°. The case ϑ = 10°, shown in Figure 6, obviously does not occur in the Arctic, and is included here just for comparison. Simulations performed for $\langle\tau\rangle$ = 15 show that the high zenith angle of the Sun is another factor which decreases the magnitudes of the biases ΔA_τ and ΔT_τ for thicker clouds. *Cahalan et al.* [1994a] demonstrated that for thin clouds over a dark underlying surface, the albedo bias magnitude is higher when the Sun is close to the horizon, opposite of what is found for thick clouds over dark surface. Our simulations for $\langle\tau\rangle$ = 1 do not contradict this tendency. However, for thin clouds, the biases due to cloud variability are negligible in the Arctic, except for a very low Sun (ϑ = 80°) where ΔT_τ = −0.012 and ΔA_τ over a nonreflective surface is 0.012. Within the analyzed ranges of parameters, magnitudes of bias contributions due to variable surface, ΔA_{As} and ΔT_{As}, decrease with solar zenith angle.

[40] Increasing the variance parameter in our model to 0.5, for example, results in considerably higher albedo and transmittance biases for a dark underlying surface (Figure 7).

However, the higher is the surface albedo the weaker is the influence of the increased cloud variability on the biases due to clouds. The albedo bias ΔA_τ is still very small for $\langle A_s\rangle$ = 0.8 and f = 0.5.

[41] The dependence of the bias on variability in surface reflectivity, expressed as σ_{As}, is shown in Figure 8. The decrease in surface variability to σ_{As} = 0.15 reduces the magnitudes of ΔA_{As} and ΔT_{As} to below 0.01. The variability in surface albedo does not visibly influence any of the biases in the case of thin clouds ($\langle\tau\rangle$ = 1).

[42] Biases in both albedo and atmospheric transmittance vary also depending on the position of thin cloud areas with respect to the most reflective stretches of the surface. Figures 9 and 10 show results of an experiment in which variability in τ in a bounded cascade cloud is correlated with the variability in the albedo of underlying surface. To obtain a positive correlation, at each cascade step a fraction of cloud water is shifted into the cell which is over the surface cell having higher albedo than the other cell, instead of being transported in a randomly chosen direction. Thus on average thicker parts of the cloud were over brighter areas of the surface. A negative correlation is obtained by transferring a portion of water toward the part of the cell with darker surface. Examples of horizontal variability in cloud LWP and surface albedo with negative and positive correlation, respectively, are given in Figure 9. Plane-parallel biases for correlated cases are shown in Figure 10. Simulations with positive correlation between cloud optical thickness and surface albedo result in considerably higher values of transmittance and lower values of albedo with respect to the average or uncorrelated situation, while simulations with negative correlation yielded opposite results. Biases may also depend on a phase shift between spatial fluctuations in surface albedo and cloud optical thickness, but this problem is beyond the scope of this work. Although the authors do not know any example of a
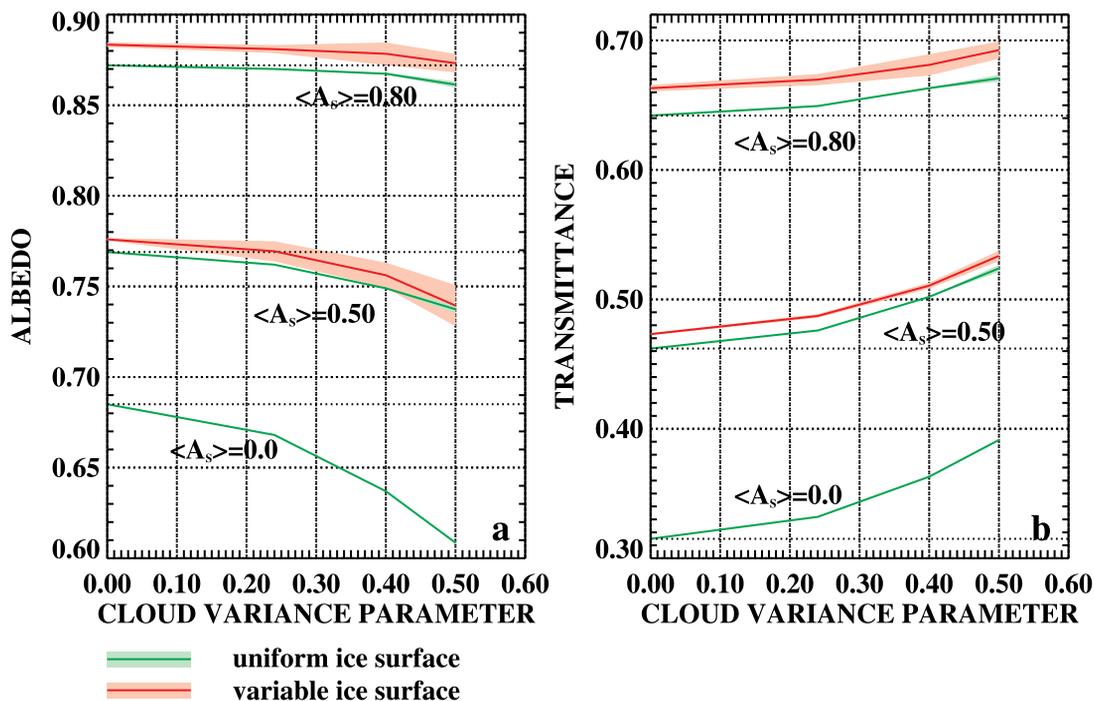
Figure 7. Biases in cloud albedo and transmittance versus variability in cloud optical thickness for the case of uniform (green line) and nonuniform (red line) surface albedo, $\langle \tau \rangle = 15$, $\vartheta = 60°$, $\sigma_{As} = 0.25$ for nonuniform case. Plane-parallel cases are for $f = 0$ and uniform surface albedo.

large scale correlation between cloud optical thickness and sea ice albedo, there are examples of shallow convective clouds that emanate from open water in leads and polynias, such as the case of 27 April 1998 from SHEBA [*Curry et al.*, 2000].

[43] Figure 11 shows dependence of the biases on cloud base height. An increase in cloud height decreases the absolute value of the surface contribution to the biases and negligibly increases the magnitude of the cloud contributions, which results in a decrease in the absolute value of the total bias. When the cloud contribution dominates over that of the surface, the total albedo bias can change sign, but this is an exception. The plane-parallel biases for high- and midlevel clouds are probably negligible.

[44] In the Arctic the character of the reflection function varies depending on the surface type. It is closest to lambertian for fresh snow and closest to mirror-like for calm water. We tested the sensitivity of the transmittance, cloud albedo and the biases to the type of surface bidirectional reflectance function and the presence of a scattering layer under the clouds. The simulation results under assumptions of mirror reflection and lambertian reflection from the surface were compared for a wide range of input parameters expected in the Arctic. No significant difference was found. On average, the mirror surface, compared to the lambertian, yields slightly lower albedo above clouds (mean = −0.0003, max difference magnitude = 0.002) and higher transmittance (mean = 0.0015, max difference = 0.004). Maximum differences were found for the thinnest clouds tested and the lowest Sun zenith angle ($\vartheta = 60°$, $\langle \tau \rangle = 5$). Respective mean differences in the biases are 0.0006 (max = 0.002) and −0.0004 (max absolute value of the difference = 0.004). Similarly, even the thickest scattering layer tested (aerosol

optical thickness under clouds 0.015, for cloud base height of only 0.150 km) did not change the results in the modeled cases ($\vartheta = 60°$, $\langle \tau \rangle = 5$ and 15).

[45] Response of the modeled cloud albedo and transmittance to perturbations in some input parameter was also computed and compared to the biases. In the majority of cases, the absolute values of the biases in transmittance and albedo are comparable to the errors due to several percent uncertainty in the mean surface albedo, or from several up to 20% in the mean optical thickness.

[46] The highest absolute values of the biases may be expected in the areas of high mean albedo with relatively high variability at larger scales, such as areas of high density of leads. Biases may also be relatively high in coastal areas, especially in the Canadian Arctic where the surface is a mosaic of sea and islands, or more precisely tundra, bare rocks, glacier ice, snow, seawater, sea ice, and melt ponds. Therefore high variability of surface albedo is expected. Moreover, correlation between surface features and cloud is more probable.

[47] In our bias estimations we considered simplified cases. We neglected the atmosphere between cloud and surface, and assumed clouds to be nonabsorbing, appropriate for visible wavelengths. Variability of both cloud optical thickness and surface albedo were simulated. Moreover, input parameters were chosen typical of visible wavelengths. Even though observed biases may vary slightly from values presented above, our findings are expected typical for shortwave radiation. In spite of methodological differences, our results are generally in agreement with results of simulations of 2 selected cases from FIRE-ACE/SHEBA done by *Benner et al.* [2001]. Both studies show that plane-parallel biases are small in the Arctic. However, our study
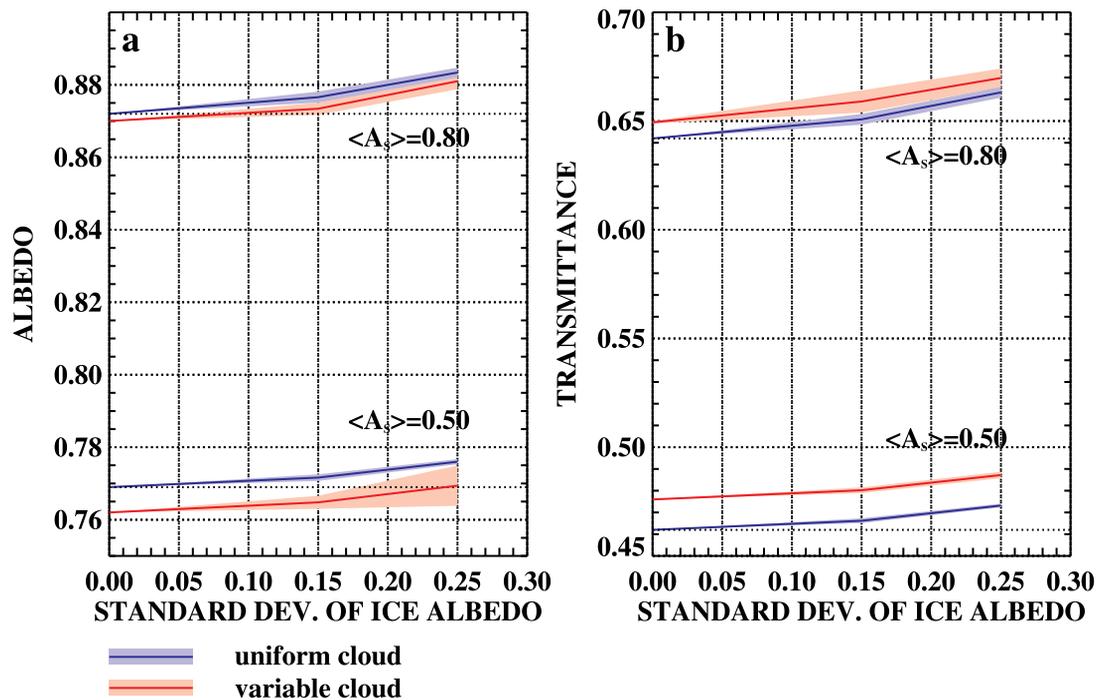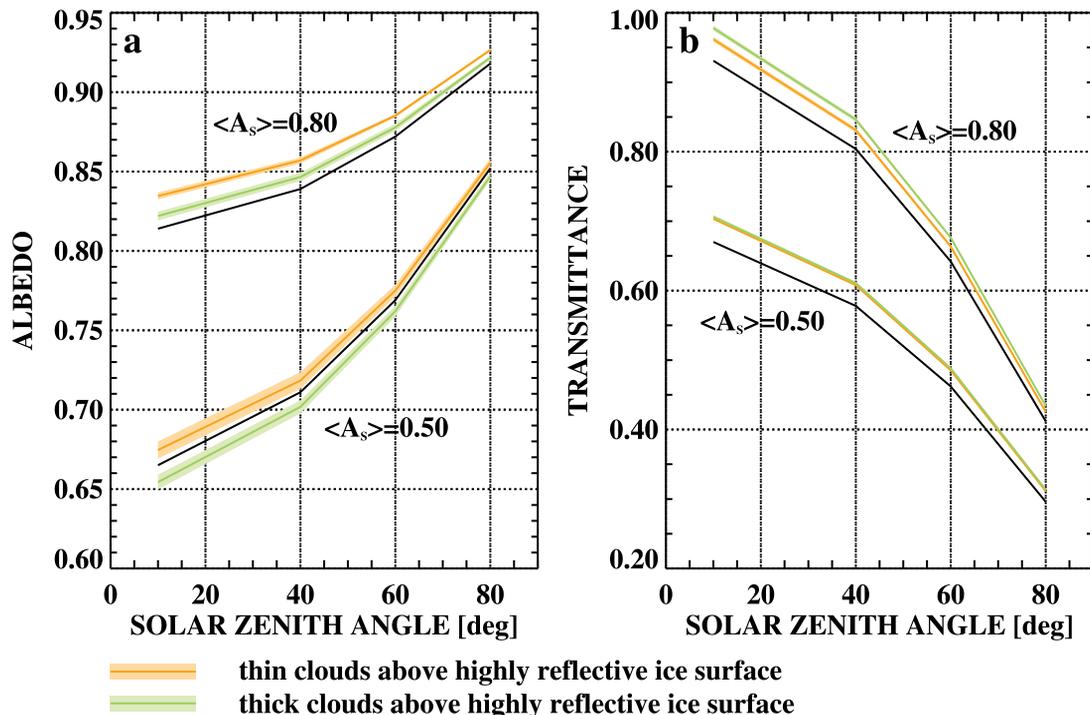
Figure 8.   Biases in cloud albedo and transmittance versus variability in surface albedo for the case of uniform (blue line) and nonuniform (red line) clouds, $\langle \tau \rangle = 15$, $\vartheta = 60°$, $f = 0.24$ for nonuniform case. Plane-parallel cases are for $\sigma_{As} = 0$ and uniform cloud.
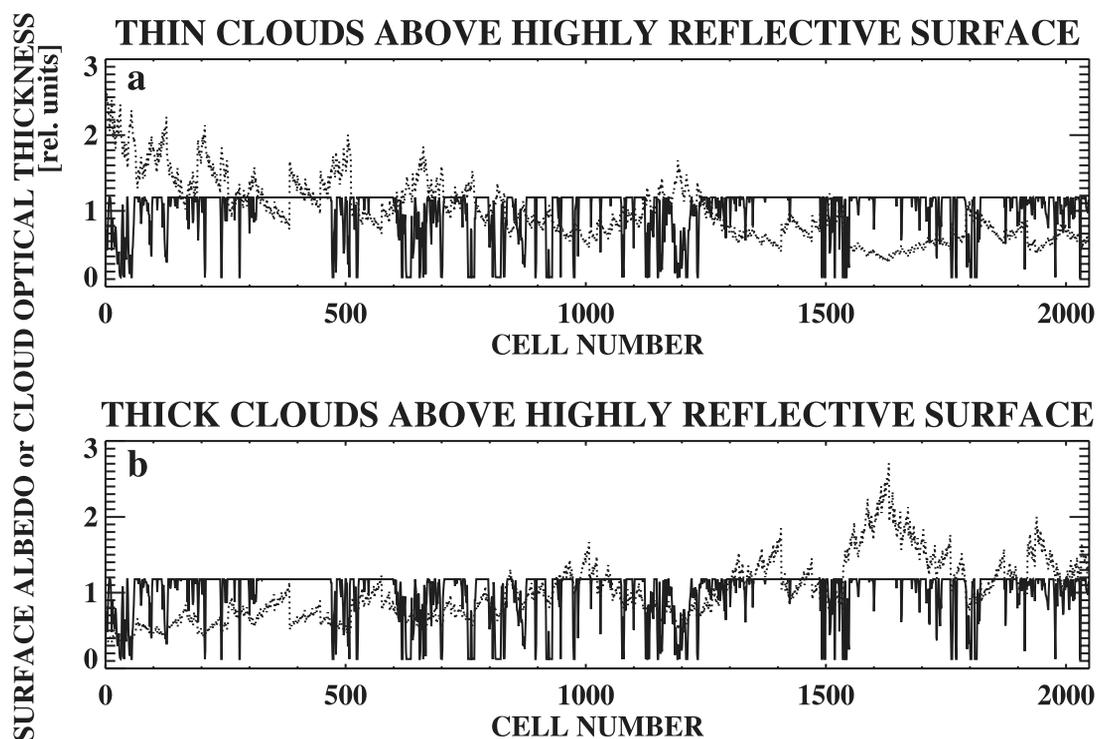
Figure 9.   Examples of cloud optical thickness (dotted line) correlated with surface albedo (solid curve) for $\langle \tau \rangle = 15$, $\langle A_s \rangle = 0.8$, $f = 0.24$, $\sigma_{As} = 0.25$:
1. a case with thin clouds more probable over more reflective parts of the surface,
2. a case with thick clouds more probable over more reflective parts of the surface.

Figure 10. Biases in cloud albedo and transmittance versus solar zenith angle for same parameter values as in Figure 6, but now with variabilities in surface albedo and cloud optical thickness correlated with each other. Cases with thin clouds more probable over more reflective parts of the surface are plotted with yellow line. Cases with thick clouds more probable over more reflective parts of the surface are plotted with green line. Black line denotes uniform cases.

also determines the dependence of the biases on the relevant parameters, and indicates conditions when biases may become significant.

[48] Contributions to the biases are discussed in Appendix A, based on simple analytical expressions for the total biases. They confirm the results of Monte Carlo simulations presented in this section.

5. Conclusions

[49] This paper employs 3D Monte Carlo radiative transfer code to simulate the expected influence of nonuniform cloud structure and nonuniform surface albedo on radiative fluxes in the Arctic atmosphere. Variability of cloud liquid water path and optical thickness are simulated using a bounded cascade fractal model. Surface albedo variability is derived from a transformed MAS scene. Cloud liquid water path and surface albedo are variable in 1 dimension. Clouds are nonabsorptive. Surface reflection function is assumed lambertian. Typical model parameters are as follows: wavelength 605 nm, cloud thickness 300 m, cloud base height 150 m (75–1200 m), cloud phase function asymmetry parameter 0.85, mean cloud optical thickness 15 (1–30), variance parameter of the bounded cascade cloud 0.24 (0.4, 0.5) (determines the variance of log(LWP)), cloud spectral or scaling parameter of the bounded cascade 0.8 (determines the exponent of the LWP power spectrum), mean surface albedo 0.0, 0.5 and 0.8, surface albedo standard deviation 0 and 0.25 (0.15), domain length 67.5 km,

minimum cell size 0.033 km, solar zenith angle 60° (10–80°). Numbers in parenthesis here show parameter values used in selected experiments.

[50] Our findings are summarized as follows:

1. Arctic clouds are optically thinner and less variable than their midlatitude counterparts. The fractal variance parameter varies from 0.1 to 0.4. This results in relatively low biases in albedo and transmittance. Plane-parallel biases due to cloud variability do not exceed 0.02 for the albedo and −0.02 for the transmittance for the modeled conditions with a dark surface.

2. A uniform reflective underlying surface diminishes the magnitude of the absolute transmittance bias due to cloud variability. This occurs because in thin cloud regions increased downwelling radiation is partly compensated by decreased cloud base albedo for upwelling from the surface, so that actual transmittance, i.e., the transmittance including contributions from multiple reflections between cloud and surface, changes little. Also, in thin cloud regions the upwelling flux from the surface partly compensates decreased cloud albedo, which results in diminishing the albedo bias over a reflective surface as well.

3. A variable reflective surface under plane-parallel clouds increases both the albedo above the clouds and the atmospheric transmittance, when compared to the plane-parallel case with the same mean value of the surface albedo. The surface properties influence the albedo and transmittance, and related biases, by multiple reflection
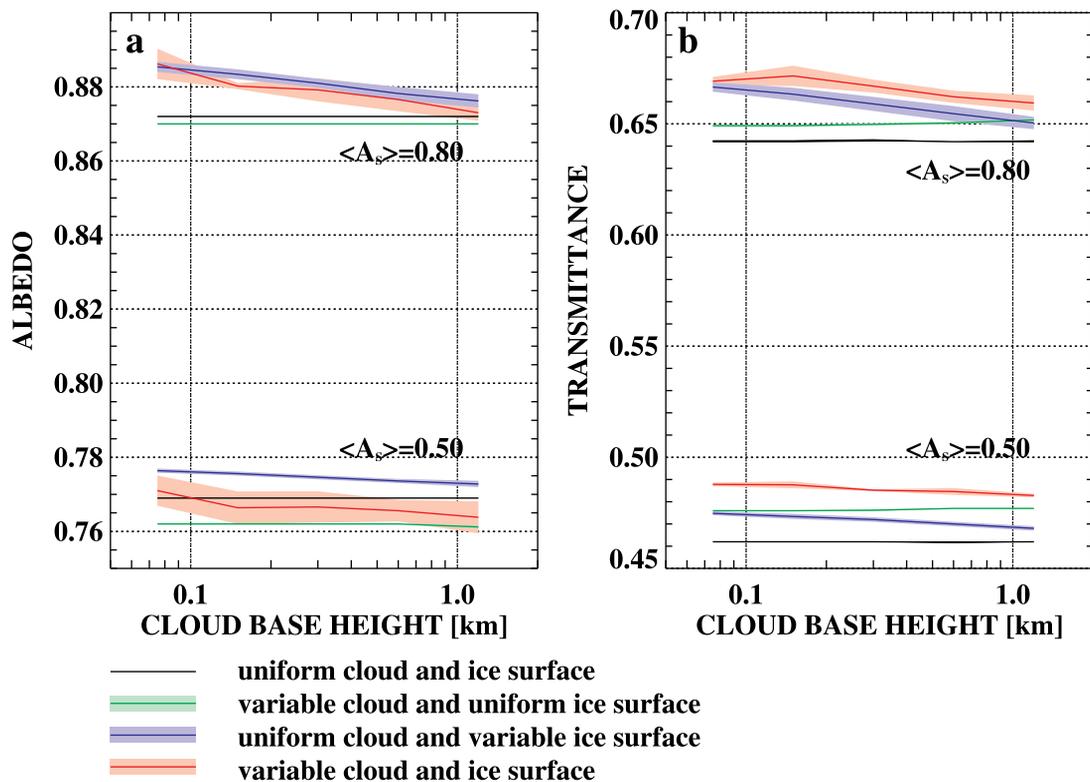
Figure 11.   Biases in cloud albedo and transmittance versus cloud base height for $\langle\tau\rangle = 15$, $f = 0.24$, $\vartheta = 60°$, $\sigma_{As} = 0.25$. Line type code is the same as in Figure 5.

between clouds and surface, which results in nonlinear hyperbolic terms in the respective equations (see Appendix A, equations (A5) and (A6)).

4. If the cloud optical thickness and the surface albedo are uncorrelated, the effective plane-parallel biases in cloud albedo and atmospheric transmittance can be estimated as the sum of the respective biases due to variability of cloud and surface. In the case of the cloud albedo, the total bias can be positive or negative depending on which contribution dominates. Its value does not exceed ±0.02. The more reflective the ice is, the less the cloud variability influences the albedo bias. In the case of transmittance, both bias contributions are negative and result in increasing the total bias magnitude, up to 0.05 for thick clouds and highly variable and reflective sea ice surface. Expressing the biases as percentages of the actual cloud albedo and transmittance, the albedo bias magnitude is less than 2% over the reflective surface, while the absolute value of the transmittance bias can exceed 10%. If there is any correlation between the cloud optical thickness and surface albedo variabilities, it influences the biases. A positive correlation, i.e., when thicker parts of the cloud are more likely to occur over brighter areas of the surface, tends to decrease albedo and increase transmittance when compared to the uncorrelated case, and thus increases the total albedo bias and increases the transmittance bias magnitude. A negative correlation results in the opposite effect, decreasing the transmittance bias magnitude and decreasing the albedo bias, which can take negative values.

5. For the modeled conditions, increased cloud optical thickness has negligible effect on the total albedo bias but

may increase the transmittance bias magnitude up to several times.

6. Low solar altitude, typical of Arctic conditions, diminishes bias magnitudes (except for very thin clouds).

7. Increasing cloud variability increases the magnitudes of cloud-related bias contributions, mainly for low $\langle A_s \rangle$. Similarly, increasing ice variability increases bias magnitudes related to surface albedo, especially for highly reflective surfaces.

8. An increase in cloud height decreases the absolute values of the surface contribution to the biases and negligibly increases the absolute values of the cloud contribution, which, for high surface albedo, results in a decrease in the absolute values of the total biases. Therefore the plane-parallel biases for high- and midlevel clouds over a highly reflective surface are negligible.

9. The biases and the fluxes (albedo above the clouds and atmospheric transmittance) are insensitive to type of surface reflection function (lambertian or mirror). Neither does a scattering layer between the clouds and the surface affect the biases in our simulations (scattering layer optical thickness up to 0.015).

[51] The biases discussed in this paper are sums of two components: the plane-parallel bias due to cloud fractal structure and the "independent pixel" bias due to net horizontal photon transport, i.e., we did not separate the contribution to the biases from the variable optical thickness of clouds and variable surface albedo by themselves, from the contributions due only net horizontal photon transport (Independent Pixel Approximation bias). Because of the multiple reflection between the clouds and the ice surface,

the relative importance of the IPA bias, due to the net 3D radiative effects, may be more important in the Arctic than over the dark subtropical oceans, where it is small compared to the plane-parallel bias [*Cahalan et al.*, 1994a]. We plan to analyze IPA biases for the wide range of the conditions expected in the Arctic. The IPA biases were calculated by *Benner et al.* [2001] for two cases from FIRE-ACE/SHEBA.

[52] In Arctic conditions surface albedo variability is typically the main factor that influences plane-parallel biases. The simple simulation of sea ice albedo variability used in this work is only our first approach. Our future work will be concentrated on developing a realistic model of 2D spatial variability of sea ice surface albedo.

[53] The present study has not resolved the question whether Arctic stratus has fractal scale invariant properties or how these may differ from midlatitude stratocumulus. *Davis et al.* [1994] and *Marshak et al.* [1997] analyzed scaling properties of liquid water distributions in marine stratocumulus and determined scaling exponents H1 and C1, measures of nonstationarity and intermittency, respectively. They found that ensemble-average nonstationarity and intermittency indices for FIRE and ASTEX clouds are close to each other, so that these measures of internal structure of marine Sc depend little on local climatology. However, *Cahalan et al.* [1995] found that cloud "gap" distributions do differ significantly between FIRE and ASTEX. Also, the present study shows significant differences between midlatitude stratocumulus and Arctic stratus, providing an example in which cloud structure depends upon the large-scale regime, a result also supported by *Cahalan and Joseph* [1989]. Further study of Arctic stratus fractal properties can be based on airborne LWC measurements from FIRE-ACE/SHEBA, and can be compared to multifractal analysis of marine stratocumulus of *Davis et al.* [1994, 1996a], and *Marshak et al.* [1997].

[54] *Lawson et al.* [2001] concluded in their paper, that the cloud particle characteristics in Arctic boundary layer clouds can be extremely inhomogeneous in both horizontal and vertical extent, e.g., in one cloud at −20 °C, spatial distances of the order of 10 km and vertical distances of 100 m separated a pocket of drizzle drops, a region with cloud drops and small unrimed particles, a region with graupel. In liquid-phase single-layered stratus near the Svalbard Archipelago, cell-like variations of LWC were accompanied by similar cell-like variations in average droplet diameter and droplet concentration [*Albers et al.*, 1999]. The observed periodicity had a basic scale of about 700 m. Similar fluctuations of scales near 1 km were observed in Arctic stratus clouds during SHEBA (21 July 1998). Droplets were bigger in areas with higher LWC (and higher droplet concentration) (D. Baumgardner, personal communication, 2001). This coupled variability evidently influenced the radiation field. This also needs further investigation.

[55] Longwave plane-parallel biases calculated by *Benner et al.* [2001] for selected FIRE-ACE/SHEBA cases were lower than their shortwave counterparts. Nevertheless, since Arctic stratus warm the surface, opposite to midlatitude stratocumulus, it is also of interest to extend this study on plane-parallel biases to the near infrared (absorbing clouds) and to longwave radiation.

Appendix A

[56] Albedo A "measured" above clouds and atmospheric (cloud) transmittance T "measured" at sea surface can be approximated by a Taylor series of the form:

$$A(X) = A(X_o) + \sum_{i=1}^{N} \frac{\partial A}{\partial x_i}(x_i - x_{0i}) + \frac{1}{2}\sum_{j=1}^{N}\sum_{i=1}^{N}\frac{\partial^2 A}{\partial x_i \partial x_j}$$
$$\cdot (x_i - x_{0i})(x_j - x_{0j}) + \ldots \qquad (A1)$$

$$T(X) = T(X_o) + \sum_{i=1}^{N} \frac{\partial T}{\partial x_i}(x_i - x_{0i}) + \frac{1}{2}\sum_{j=1}^{N}\sum_{i=1}^{N}\frac{\partial^2 T}{\partial x_i \partial x_j}$$
$$\cdot (x_i - x_{0i})(x_j - x_{0j}) + \ldots \qquad (A2)$$

where $X = [x_1, x_2,\ldots,x_n]$. In the one-dimensional case, $N = 1$, $X_0 = [\langle\tau\rangle]$ and $X = [\tau]$, or $X_0 = [\langle A_s\rangle]$ and $X = [A_s]$. In 2D, $X_0 = [\langle\tau\rangle, \langle A_s\rangle]$, $X = [\tau, A_s]$.

[57] In this appendix biases we adopt the independent pixel approximation (IPA) approach, i.e., we neglect horizontal transfer of photons between pixels. However, the horizontal transport is included in Monte Carlo simulations.

[58] After averaging (A1) and (A2) over the domain, which eliminates the linear term, we can express the plane-parallel bias for albedo and transmittance as follows:

$$\Delta A_{\tau,A_s} = -\frac{1}{2}\frac{\partial^2 A}{\partial\tau^2}\bigg|_{\tau=\langle\tau\rangle, A_s=\langle A_s\rangle}\cdot\sigma_\tau^2 - \frac{1}{2}\frac{\partial^2 A}{\partial A_s^2}\bigg|_{\tau=\langle\tau\rangle, A_s=\langle A_s\rangle}$$
$$\cdot\sigma_{A_s}^2 - \frac{\partial^2 A}{\partial\tau\partial A_s}\bigg|_{\tau=\langle\tau\rangle, A_s=\langle A_s\rangle}\cdot\sigma_\tau\sigma_{A_s}C_{\tau,A_s} - \ldots \qquad (A3)$$

$$\Delta T_{\tau,A_s} = -\frac{1}{2}\frac{\partial^2 T}{\partial\tau^2}\bigg|_{\tau=\langle\tau\rangle, A_s=\langle A_s\rangle}\cdot\sigma_\tau^2 - \frac{1}{2}\frac{\partial^2 T}{\partial A_s^2}\bigg|_{\tau=\langle\tau\rangle, A_s=\langle A_s\rangle}$$
$$\cdot\sigma_{A_s}^2 - \frac{\partial^2 T}{\partial\tau\partial A_s}\bigg|_{\tau=\langle\tau\rangle, A_s=\langle A_s\rangle}\cdot\sigma_\tau\sigma_{A_s}C_{\tau,A_s} - \ldots \qquad (A4)$$

σ^2 and C_{τ,A_s} stand for variance and correlation coefficient, respectively. The first terms are contributions to the albedo and transmittance biases due to cloud variability, the second terms are contributions due to surface albedo variability. The total bias in cloud albedo and transmittance, i.e., the sum of the respective biases due to cloud and surface variability is modified by the correlation term. The correlation terms equal zero if cloud and surface variabilities are uncorrelated.

[59] To assess the sign of the bias we neglect higher terms than the second derivatives. *Cahalan* [1994] and *Cahalan et al.* [1994a] showed that the albedo bias for clouds over a nonreflective ocean, expressed by a Taylor expansion with respect to $\langle$LWP$\rangle$ converged slowly, so higher terms of the series should be taken into account. Faster convergence was found for the expansion of A expressed as a function of log(LWP). Here we consider only the linear case, as our goal is not to estimate the exact bias values but only to generally discuss the character of each bias contribution in (A3) and (A4) to the total plane-parallel bias for transmittance and albedo.

[60] For clouds over a reflective surface, the actual (measured, apparent) cloud transmittance measured at the surface and cloud albedo measured above clouds can be expressed as follows:

$$A = A_0(\mu_0) + \frac{A_s T_0(\mu_0) T_0^D}{1 - A_s A_0^D} \qquad (A5)$$

$$T = \frac{T_0(\mu_0)}{1 - A_s A_0^D} \qquad (A6)$$

where $A_0(\mu_0)$ and $T_0(\mu_0)$ are the shortwave cloud albedo and transmittance for a cloud layer above a dark surface. A_0^D and T_0^D denote cloud albedo and transmittance for diffuse flux, such as the flux reflected from the surface.

[61] If cloud is nonabsorbing then:

$$A_0^D + T_0^D = 1 \qquad (A7)$$

$$A_0(\mu_0) + T_0(\mu_0) = 1 \qquad (A8)$$

[62] In order to make a quick estimate of the biases, we assume that both cloud transmittance and albedo for solar and diffused radiation are equal and can be expressed by the following simplified relations [*Lenoble*, 1985; *Cahalan et al.*, 1994a]:

$$A_0^D = A_0(\mu_0) = \frac{\gamma\tau}{1 + \gamma\tau} \qquad (A9)$$

$$T_0^D = T_0(\mu_0) = \frac{1}{1 + \gamma\tau} \qquad (A10)$$

In fact, γ is a function of the incident radiation angle and the cloud phase function. Therefore the albedos and transmittances for upward (diffuse) and downward solar flux differ from each other even for a uniform cloud because of different angular radiance distributions in the upward and downward fluxes. However, the assumptions we made are sufficient for our purposes.

[63] Substituting (A9) and (A10) into (A5) and (A6) we obtain:

$$A = \frac{\gamma\tau[1 + \gamma\tau(1 - A_s)] + A_s}{(1 + \gamma\tau)[1 + \gamma\tau(1 - A_s)]} \qquad (A11)$$

$$T = \frac{1}{1 + \gamma\tau(1 - A_s)} \qquad (A12)$$

[64] Derivatives of (A3) and (A4) can be calculated analytically from (A11) and (A12). The term

$$-\frac{\partial^2 A}{\partial\tau^2} = \frac{2\gamma^2}{(1 + \gamma\tau)^3} + \frac{\gamma^2 A_s^2}{(1 + \gamma\tau)^3[1 + \gamma\tau(1 - A_s)]^2}$$
$$- \frac{2\gamma^2 A_s(1 - A_s)}{[1 + \gamma\tau(1 - A_s)]^3} - \frac{3\gamma^2 A_s}{(1 + \gamma\tau)^3[1 + \gamma\tau(1 - A_s)]}$$
$$- \frac{\gamma^2 A_s(1 - A_s)}{(1 + \gamma\tau)^2[1 + \gamma\tau(1 - A_s)]^2} \qquad (A13)$$

is positive except for high surface albedo values when it becomes small and negative. The bias contribution due to

clouds, ΔA_τ, (Figure 5) is always positive. However, we must remember that $-\partial^2 A \partial\tau^2$ is only the first nonzero term of the expansion and higher order terms may modify the sign of the bias. The term

$$-\frac{\partial^2 T}{\partial\tau^2} = \frac{-2\gamma^2(1 - A_s)^2}{[1 + \gamma\tau(1 - A_s)]^3} \qquad (A14)$$

is always negative, like ΔT_τ determined by the Monte Carlo simulations (Figure 5). The term

$$-\frac{\partial^2 A}{\partial A_s^2} = \frac{-2\gamma\tau}{[1 + \gamma\tau(1 - A_s)]^3} \qquad (A15)$$

is always negative and its magnitude takes the maximum values for high A_s and high τ. In the case of high surface albedo, the albedo bias magnitude due to variability in surface albedo, simulated by the Monte Carlo model, is also maximum for high τ. However, in the case of low A_s, the bias magnitude maximum is observed for $\tau = 5 - 10$ (compare Figure 5).

[65] The term

$$-\frac{\partial^2 T}{\partial A_s^2} = \frac{-2(\gamma\tau)^2}{[1 + \gamma\tau(1 - A_s)]^3} \qquad (A16)$$

is always negative and its magnitude takes its maximum values for high A_s and high τ. For low A_s or low τ the absolute value of this term is small. In the Monte Carlo simulations the bias magnitude also increases as A_s and τ increase. The term

$$-\frac{\partial^2 A}{\partial\tau\partial A_s} = \frac{2\gamma(1 - A_s)}{[1 + \gamma\tau(1 - A_s)]^3} \qquad (A17)$$

is always positive and takes its highest values for small A_s and τ. For low values of A_s, it depends manly on τ, while for high values of A_s it decreases with increasing A_s. In our Monte Carlo simulation (Figure 10), the influence of a correlation between cloud optical thickness and surface albedo variability is positive (i.e., positive correlation results in the positive bias component) and stronger for $A_s = 0.5$ than it is for $A_s = 0.8$.

[66] The term

$$-\frac{\partial^2 T}{\partial\tau\partial A_s} = \frac{\gamma[\gamma\tau(1 - A_s) - 1]}{[1 + \gamma\tau(1 - A_s)]^3} \qquad (A18)$$

is negative except for cases with low τ and high A_s when it can be positive (but close to zero). Its magnitude takes its highest values for high A_s and small τ. In our Monte Carlo simulation for $\tau = 15$ $\Delta T_{\tau,As}$ is practically independent of a correlation between cloud optical thickness and surface albedo variability for $A_s = 0.5$, while for $A_s = 0.8$ the influence of the correlation term is visible, which is in agreement with behavior of (A18) (compare Figure 10).

References

Albers, F., A. Reuter, U. Maixner, L. Levkov, E. Raschke, and I. Sednev, Horizontal inhomogeneities in clouds and their effect on remote particle measurements, *Phys. Chem. Earth, Part B*, 24, 197–202, 1999.

Allison, I., R. E. Brandt, and S. G. Warren, East Antarctic sea ice: Albedo, thickness, distribution, and snow cover, *J. Geophys. Res.*, 98, 12,417–12,429, 1993.

Arnold, G. T., S-T Tsay, M. D. King, J. Y. Li, and P. F. Soulen, Airborne spectral measurements of surface-atmosphere anisotropy for arctic sea ice and tundra, *Int. J. Remote Sens.*, in press, 2002.

Barker, H. W., and J. A. Davies, Solar radiative fluxes for broken cloud fields above reflecting surfaces, *J. Atmos. Sci.*, 49, 749–761, 1992a.

Barker, H. W., and J. A. Davies, Solar radiative fluxes for stochastic, scale-invariant broken cloud fields, *J. Atmos. Sci.*, 49, 1115–1126, 1992b.

Benner, T. C., J. A. Curry, and J. O. Pinto, Radiative transfer in the summertime Arctic, *J. Geophys. Res.*, 106, 15,173–15,183, 2001.

Byrne, R. N., R. C. J. Somerville, and B. Subasilar, Broken-cloud enhancement of solar radiation absorption, *J. Atmos. Sci.*, 53, 878–886, 1996.

Cahalan, R. F., Overview of fractal clouds, in *RSRM'87: Advances in Remote Sensing Retrieval Methods*, edited by A. Deepak, H. E. Fleming, and J. S. Theon, 371–388, A. Deepak, Hampton, Va., 1989.

Cahalan, R. F., Bounded cascade clouds: Albedo and effective thickness, *Nonlinear Process. Geophys.*, 1, 156–167, 1994.

Cahalan, R. F., and J. H. Joseph, Fractal statistics of cloud fields, *Mon. Weather Rev.*, 117, 261–272, 1989.

Cahalan, R. F., and J. B. Snider, Marine stratocumulus structure, *Remote Sens. Environ.*, 28, 95–107, 1989.

Cahalan, R. F., W. Ridgway, W. J. Wiscombe, T. L. Bell, and J. B. Snider, The albedo of fractal stratocumulus clouds, *J. Atmos. Sci.*, 51, 2434–2455, 1994a.

Cahalan, R. F., W. Ridgway, W. J. Wiscombe, S. Gollmer, and Harshvardhan, Independent pixel and Monte Carlo estimates of stratocumulus albedo, *J. Atmos. Sci.*, 51, 3776–3790, 1994b.

Cahalan, R. F., D. Silberstein, and J. B. Snider, Liquid water path and plane-parallel albedo bias during ASTEX, *J. Atmos. Sci.*, 52, 3002–3012, 1995.

Curry, J., W. B. Rossow, D. Randall, and J. L. Schramm, Overview of Arctic clouds and radiation characteristics, *J. Clim.*, 9, 1731–1764, 1996.

Curry, J. A., et al., FIRE Arctic Clouds Experiment, *Bull. Am. Meteorol. Soc.*, 81, 5–29, 2000.

Davis, A., A. Marshak, W. J. Wiscombe, and R. F. Cahalan, Multifractal characterizations of nonstationarity and intermittency in geophysical fields: Observed, retrieved, or simulated, *J. Geophys. Res.*, 99, 8055–8072, 1994.

Davis, A., A. Marshak, W. J. Wiscombe, and R. F. Cahalan, Multifractal characterizations of intermittency in nonstationary geophysical signals and fields—A model-based perspective on ergodicity issues illustrated with cloud data, in *Current Topics in Nonstationary Analysis*, edited by G. Treviño, 97–158, World-Sci., River Edge, N. J., 1996a.

Davis, A., A. Marshak, W. J. Wiscombe, and R. F. Cahalan, Scale invariance of liquid water distributions in marine stratocumulus, part I, Spectral properties and stationary issues, *J. Atmos. Sci.*, 53, 1538–1558, 1996b.

Davis, A., A. Marshak, R. F. Cahalan, and W. J. Wiscombe, The Landsat scale break in stratocumulus as a three-dimensional radiative transfer effect: Implications for cloud remote sensing, *J. Atmos. Sci.*, 54, 241–260, 1997.

Davis, A. B., A. Marshak, H. Gerber, and W. J. Wiscombe, Horizontal structure of marine boundary layer clouds from centimeter to kilometer scales, *J. Geophys. Res.*, 104, 6123–6144, 1999.

Dong, X. Q., G. G. Mace, P. Minnis, and D. F. Young, Arctic stratus cloud properties and their effect on the surface radiation budget: Selected cases from FIRE ACE, *J. Geophys. Res.*, 106, 15,297–15,312, 2001.

Gage, S. K., and D. G. Nastrom, Theoretical interpretation of atmospheric wavenumber spectra of wind and temperature observed by commercial aircraft during GASP, *J. Atmos. Sci.*, 43, 729–740, 1986.

Grenfell, T. C., and D. K. Perovich, Spectral albedos of sea ice and incident solar irradiance in the southern Beaufort Sea, *J. Geophys. Res.*, 89, 3573–3580, 1984.

Grenfell, S. G., S. G. Warren, and P. C. Mullen, Reflection of solar radiation by the Antarctic snow surface at ultraviolet, visible and near-infrared wavelengths, *J. Geophys. Res.*, 99, 18,669–18,684, 1994.

Herman, G. F., and J. A. Curry, Observational and theoretical studies of solar radiation in the Arctic stratus clouds, *J. Clim. Appl. Meteorol.*, 23, 5–24, 1984.

Hignett, P., and P. Taylor, The radiative properties of inhomogeneous boundary layer cloud: Observations and modeling, *Q. J. R. Meteorol. Soc.*, 122, 1341–1363, 1996.

Hobbs, P. V., and A. L. Rangno, Microstructure of low and middle-level clouds over the Beaufort Sea, *Q. J. R. Meteorol. Soc.*, 124, 2035–2071, 1998.

King, M., et al., Airborne scanning spectrometer for remote sensing of cloud, aerosol, water vapour, and surface properties, *J. Atmos. Ocean. Technol.*, 13, 777–794, 1996.

Kraichnan, R. H., Inertial ranges in two-dimensional turbulence, *Phys. Fluids*, 10, 1417–1423, 1967.

Lawson, R. P., B. A. Baker, C. G. Schmitt, and T. L. Jensen, An overview of microphysical properties of Arctic clouds observed in May and July 1998 during FIRE.ACE, *J. Geophys. Res.*, 106, 14,989–15,014, 1998.

Lenoble, J., (Ed.), *Radiative Transfer in Scattering and Absorbing Atmospheres: Standard Computational Procedures*, 300 pp., A. Deepak, Hampton, Va., 1985.

Makshtas, A. P., E. L. Andreas, P. N. Svyaschennikov, and V. F. Timachev, Accounting for clouds in sea ice models, *Atmos. Res.*, 52, 77–113, 1999.

Marchuk, G., G. Mikhailov, M. Nazaraliev, R. Darbinjan, B. Kargin, and B. Elepov, *The Monte Carlo Methods in Atmospheric Optics*, 208 pp., Springer-Verlag, New York, 1980.

Marshak, A., A. Davis, R. Cahalan, and W. Wiscombe, Bounded cascade models as nonstationary multifractals, *Phys. Rev. E*, 49, 55–69, 1994.

Marshak, A., A. Davis, W. Wiscombe, and G. Titov, The verisimilitude of the independent pixel approximation used in cloud remote sensing, *Remote Sens. Environ.*, 52, 71–78, 1995.

Marshak, A., A. Davis, W. J. Wiscombe, and R. F. Cahalan, Scale invariance in liquid water distributions in marine stratocumulus, part II, Multifractal properties and intermittency issues, *J. Atmos. Sci.*, 54, 1423–1444, 1997.

Perovich, D. K., Light reflection from sea ice during the onset of melt, *J. Geophys. Res.*, 99, 3351–3359, 1994.

Perovich, D. K., Observations of the polarization of light reflected from sea ice, *J. Geophys. Res.*, 103, 5563–5575, 1998.

Perovich, D. K., T. C. Grenfell, B. Light, J. A. Richter-Menge, M. Sturm, W. B. Tucker, III H. Eicken, G. A. Maykut, and B. Elder, *SHEBA: Snow and Ice studies*, version 1, [CD-ROM], 1999a.

Perovich, D. K., et al., Year on ice gives climate insights, *Eos Trans. AGU*, 80, 481–484, 1999b.

Pinto, J. O., and J. A. Curry, Role of radiative transfer in the modeled mesoscale development of summertime arctic stratus, *J. Geophys. Res.*, 102, 13,861–13,872, 1997.

Pinto, J. O., J. A. Curry, and C. W. Fairall, Radiative characteristics of the Arctic atmosphere during spring as inferred from ground-based measurements, *J. Geophys. Res.*, 102, 6941–6952, 1997.

Pinto, J. O., J. A. Curry, and J. M. Intrieri, Cloud-aerosol interactions during autumn over Beaufort Sea, *J. Geophys. Res.*, 106, 15,077–15,097, 2001.

Ricchiazzi, P., and C. Gautier, Investigation of the effect of surface heterogeneity and topography on the radiation environment of Palmer Station, Antarctica, with a hybrid 3-D radiative transfer model, *J. Geophys. Res.*, 103, 6161–6176, 1998.

Shupe, M. D., T. Uttal, S. Y. Matrosov, and A. S. Frisch, Cloud water contents and hydrometeor sizes during the FIRE Arctic Clouds Experiment, *J. Geophys. Res.*, 106, 15,015–15,028, 2001.

Soulen, P. F., M. D. King, S.-C. Tsay, G. T. Arnold, and J. Y. Li, Airborne spectral measurements of surface-atmosphere anisotropy during the SCAR-A, Kuwait Oil Fire, and TARFOX experiments, *J. Geophys. Res.*, 105, 10,203–10,218, 2000.

Stamnes, K., S.-C. Tsay, W. Wiscombe, and K. Jayaweera, Numerically stable algorithm for discrete-ordinate-method radiative transfer in multiple scattering and emitting layered media, *Appl. Opt.*, 27, 2502–2509, 1998.

Stamnes, K., S.-C. Tsay, and I. Laszlo, *DISORT, a general-purpose Fortran program for discrete-ordinate method radiative transfer in scattering and emitting layered media: Documentation and methodology, ver. 1.1.*, 2000.

Tsay, S.-C., and K. Jayaweera, Physical characteristics of Arctic stratus clouds, *J. Clim. Appl. Meteorol.*, 23, 584–596, 1984.

Westwater, E. R., Y. Han, M. D. Shupe, and S. Y. Matrosov, Analysis of integrated cloud liquid and precipitable water vapor retrievals from microwave radiometers during SHEBA, *J. Geophys. Res.*, 106, 32,019–32,030, 2001.

Zhang, T., K. Stamnes, and S. A. Bowling, Impact of clouds on surface radiative fluxes and snowmelt in the Arctic and subarctic, *J. Clim.*, 9, 2110–2123, 1996.

Zuev, V. E., and G. Titov, Radiative transfer in cloud fields with random geometry, *J. Atmos. Sci.*, 52, 176–190, 1995.

R. F. Cahalan, Goddard Space Flight Center, NASA, Greenbelt, MD 20771, USA.

A. Rozwadowska, Institute of Oceanology, Polish Academy of Sciences, Powstancow Warszawy 55, 81-712 Sopot, Poland. (ania@iopan.gda.pl)